Fluidized Landsliding Phenomenon on Volcanic Ash Slope during Heavy Rainfall: A Case Study of Izu Oshima Landslides

Gonghui WANG(1) and Yao JIANG(2)

(1) Disaster Prevention Research Institute, Kyoto University, Japan
E-mail:wanggh@landslide.dpri.kyoto-u.ac.jp
(2) Graduate School of Science, Kyoto University, Japan

Abstract

On Oct. 16, 2013, catastrophic shallow landslides were triggered on a wide area of the west-side hill slopes in Izu-Oshima Island, Japan, by the heavy rainfall accompanying Typhoon Wipha. The displaced landslide materials traveled long distance with rapid movement, resulting in 36 dead, 3 missing, and 46 buildings being completely destroyed on the downstream area of Motomachi area. To understand the initiation and movement mechanisms of these shallow landslides, we took sample from the source areas and examined the shear behavior of these samples under partially drained or undrained condition. We also triggered landslides within soil layers made up of these samples by rainfall in a flume, and examined the variation of soil moisture, pore-water pressure and landslide movement with the introduction of rainwater. Test results showed that high pore-water pressure can be built up and maintained within the displaced landslide material, and then elevate the landslide mobility.

Keywords: shallow landslides, heavy rainfall, mobility, liquefaction, tephra slope

1. Introduction

Typhoon Wipha started as a tropical storm on 9 October 2013 over the sea near the island of Guam, and strengthened on October 11, and later on October 12, 2013, it intensified into a typhoon. Typhoon Wipha weakened as it skirted Japan's eastern coastline on October 15 as the ocean waters surrounding the typhoon began to cool, and reached extra-tropical status late on October 16, and finally disappeared on the north-east of Pacific Ocean.

Typhoon Wipha dumped very heavy rain and whipped up strong winds in many areas of East Japan. The 24-hour amount of rainfall through 8:20 a.m. in Oshima on Oct. 16 totaled 824 mm, setting up a new record. This daily precipitation is equivalent to more than twice the amount that Oshima had in all of October in an average year. The maximum hourly rainfall reached 125 mm. Also a maximum wind velocity was recorded as 35 m/s. As a result of the rainfall, several landslides were triggered in the thin volcanic ash layer of hillside surface. Among them, a massive one from an area perched above the Motomachi district traveled approximately 2.2 km, demolished a large area of the town, caused 36 fatalities and left 3 others missing, and destroyed more than 40 buildings.

Fig. 1 Landslides in Izu Oshima during Typhoon Wipha, 2013 (after Geospatial Information Authority of Japan, 2013). S: sampling point.

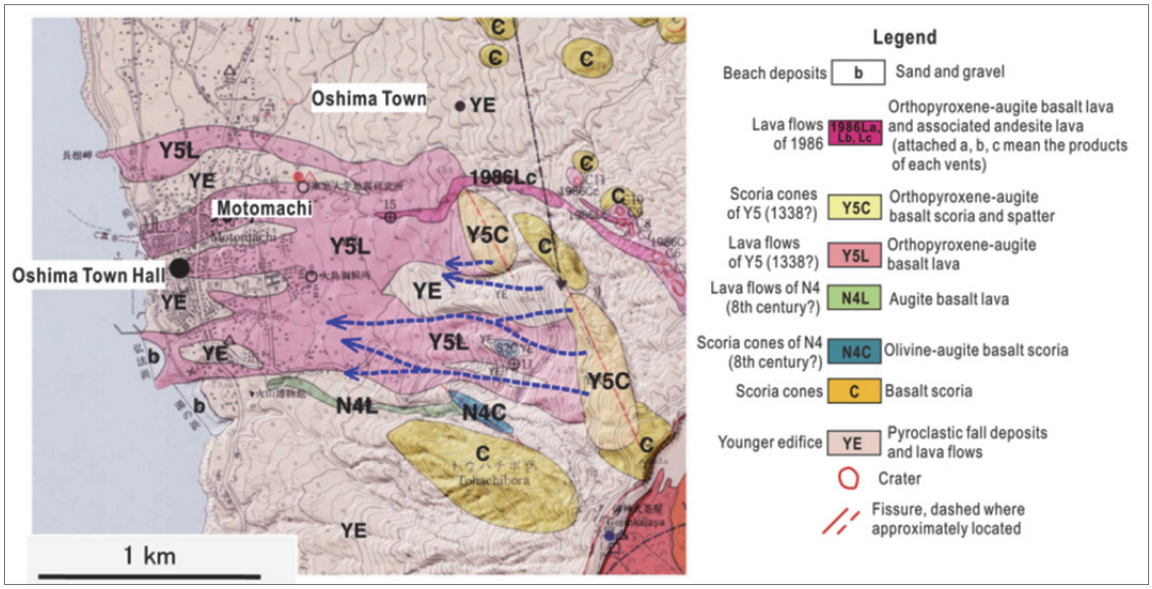

Fig. 3 Geological map of the landslide area (after Kawanabe (1998) and Geological Survey of Japan (2013)

Owning to its high mobility and the characters of its traveling path and deposits, we describe the landslide at Motomachi as a debris avalanche, following the classification of landslide type presented by Hungr et al. (2001) (hereinafter termed as MDA). Understanding the initiation and movement mechanisms of the MDA is of great importance to the prevention or mitigation of similar type of landslides in volcanic deposits under extreme weather conditions. To achieve this, we conducted detailed field survey on those landslides in Izu Oshima Island triggered by Typhoon Wipha, and took samples from the source area of MDA. We examined the undrained or partially drained shear behavior of these samples in saturated state by ring shear tests. We also triggered a series of landslides in an instrumented flume by sparkling water to examine the hydraulic condition under which the slope instability was triggered, and also to examine the post failure phenomena of the displaced materials.

2. Landslides in Izu Oshima

Izu Oshima is an active volcano about 100 km SSW of Tokyo and east of Izu Peninsula in the NW Pacific Ocean. Many eruptive activities have occurred in the past. Most recently, a serious fissure eruption occurred on 21 November 1986 and forced all the residents of the island to evacuate for the first time. The outline of the island is oval shape elongated in NNW-SSE direction with length about 15 km and width about 9 km. Mt. Miharayama is the highest point of the island (764 m above the sea level). Motomachi, as the main district on the island, is located on the west side.

With the approach and passing of Typhoon Wipha, rainfall started on October 15 in Oshima and became stronger gradually. During the next day as Wipha moved towards the north-northwest it dumped very heavy rain. In the town of Oshima, an hourly rainfall total of 100 mm and a 24-hour total of 824 mm were recorded (Fig. 2). As a result, several shallow landslides over large areas were triggered in the thin volcanic ash layer on the hillsides perched above the town.

These landslides are located on the outer slope of the caldera wall that was formed during the eruption of 1,300-1,500 year ago and featured by sharp slope. In the landslide area a crater was formed due to the fissure eruption in the era of 1330 (Y5) (Fig. 3). The lava of this eruption was covered by tephra (scoria and ash) layers that came from 4 times of eruption (Y4-Y1) (Fig. 4). These tephra layers have a thickness reaching several meters in maximum and show stratifications nearly parallel to the slope surfaces.

The landslides are mainly localized on two catchments where the slopes are steeper than 20 degrees and the relief within a square of 1km×1km is about 200-300m. The most upper part of the failed slope originated on the elevation of 450 m. The failures on the upper slope of the road were about 10-40 m wide, and widened to 50-100m on the slope below the road, and finally combined as a whole with a width of about 250m on the elevation of 300-400m.

Our field investigation revealed that the thickness of the displaced landslide material on the source area was about 70-120 cm. The source area of the biggest one involved a failure area of about 0.13 km^2. The outcropped sliding surfaces are loess, above which is the tephra of Y2 formed during the 1684 volcanic eruption. According to Terajima et al. (2015), the permeability of this loess layer ranges approximately from 10^{-4} to 10^{-5} cm/s, while that of the overlaying

tephra is about 10^{-2}~10^{-3} cm/s. As a possible mechanism on the initiation of the shallow landslide, we inferred that this permeability contrast enabled the formation of a perched saturated soil layer with increasing water table, and finally resulted in the instability of the tephra layers. We also inferred that the displaced materials started as slide and then transformed into flow.

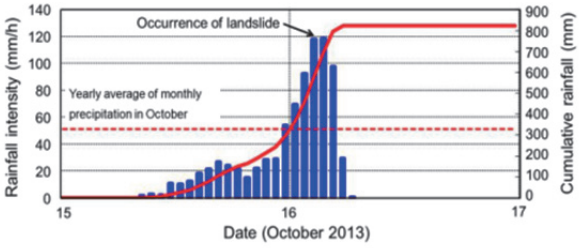

Fig. 2 Rainfall in Izu-Oshima on 14-16 October 2014

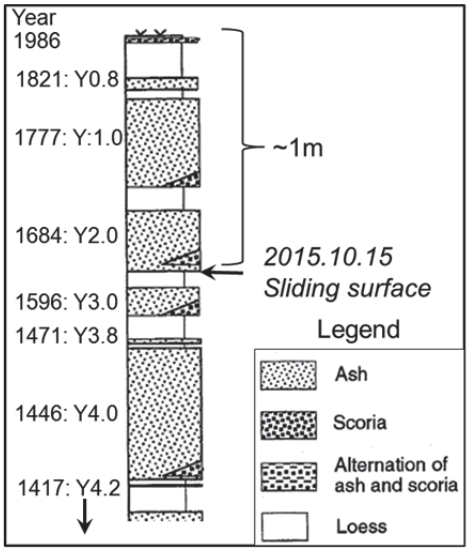

Fig. 4 A standard columnar section of tephra and loess in Motomachi area (after Koyama and Hayakawa, 1996)

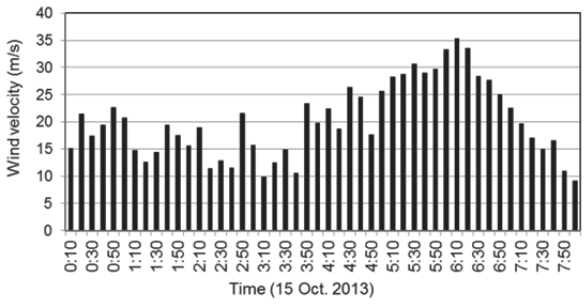

Fig. 5 Wind velocities on 16 October 2014

Trees on the hillside might have also played an important role in both triggering the slope instability and elevating the destructive capacity of the displaced materials. On October 16, wind velocity reached about 35 m/s (Fig. 5). Those trees (about 20 m high in average with roots less than 70 cm below the ground surface) might have suffered strong wind throw, which could enforce the instability of the shallow slope. In addition, a huge number of trees moving downhill together with the displaced materials could greatly enforce the destructive power to the houses on its traveling path. The driftwoods also blocked the downstream bridges, causing floods and resulting in further loss of life and property damage. It is noted that during our field survey we monitored the ground vibration and wind velocity on the forest of hillside slope aiming at understanding the possible effect of wind throw on the instability. Although detailed analyses of these monitored data are still in progress, our field monitor by video showed that the wind throw of trees may contribute greatly to the initiation of shallow landslide on the hillside.

3. Methods

To examine the initiation and movement mechanisms, we took samples from different soil layers above the sliding surface on the source area. Our sampling point has a soil layer of 90 cm thick above the sliding surface (on the upper part of the loess layer). We took samples from the loess layer (Sample LL), from the tephra layer of coarse volcanic sand immediately above the loess layer (Sample VS), and also from the tephra layers of silty-fine volcanic sand locating 10 and 20 cm (Sample VL1 and VL2) above sample VS, respectively. We also used the samples (two tons) that were collected from the deposited area in Motomachi town for flume tests.

A ring shear apparatus was used to examine the shear behavior of the samples taken from the source area. This apparatus, which has a shear box with 120 mm inner diameter, 180 mm outer diameter, 115 mm height, and a maximum shear velocity of 10 cm/s, enables shearing at different types of loadings under either drained or undrained conditions.

The specimens in ring shear tests were prepared by pouring oven-dried samples into the shear box in layers and compacting the layers to different densities (Ishihara, 1993). All saturated test specimens were saturated by CO_2 and de-aired water. For undrained shear tests, all specimens were consolidated under a given normal stress and then sheared to residual state using a shear-speed-controlled method. In partially drained conditions, dissipation of generated pore-water pressure from the shear zone was key to the after-main-shock movement of the displaced landslide mass. To examine the possible role of dissipation of pore-water pressure, shear tests were also performed under partially drained conditions on a water-saturated sample and a M15-fluid-saturated sample. Note that M15-fluid refers the viscosity of the Metolose fluid is 15 times that of water. All the ring shear tests are summarized in Tables 1-3.

A flume (200 cm long, 25.5 cm wide and 50 cm high) with transparent sides was used to study the infiltration process of rainwater through examining the moisture variation within the volcanic ash layers, and also to examine the post failure behavior of the shallow landslides due to the introduction of rainfall (Fig. 6). We glued the same soils as the sample to the surface of the flume base to assure the same friction between the particles of sample and the base of the flume as of that of sample inside the flume.

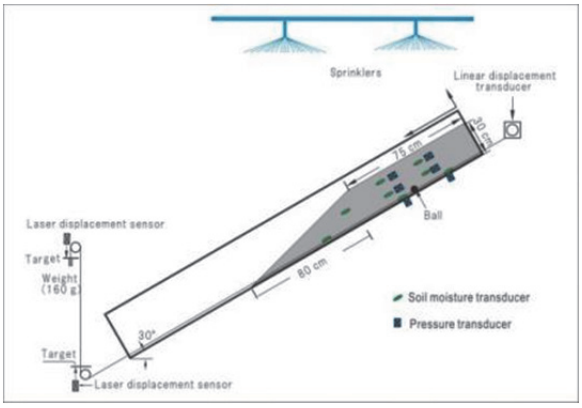

Fig. 6 Layout of the flume test

Table 1 Densities of tested samples for measuring the friction angle

sample	Normal stress (kPa)	Density (g/cm^3)
VL1 (Depth: 70-80 cm)	40	1.24
	60	1.32
	80	1.35
	100	1.37
VS (Depth: 80-90 cm)	40	1.33
	60	1.39
	80	1.42
	100	1.43
LL (Depth: 90-100 cm)	40	1.14
	60	1.23
	80	1.27
	100	1.30

Table 2: Conditions of undrained tests

sample	Normal stress (kPa)	Density (g/cm^3)
LL (Depth: 90-100 cm)	60	1.19
VS (Depth: 80-90 cm)	60	1.33

Table 3: Conditions of partially drained tests

sample	Normal stress (kPa)	Density (g/cm^3)
LL (Depth: 90-100 cm)	60	1.21
VL1 (Depth: 80-90 cm)	60	1.36
VS (saturated by M15) (Depth: 80-90 cm)	60	1.44

As shown in Fig. 6, pore-water pressure (PWP) and soil moisture were measured at 7 locations. In the place immediately close to the location of PWP in the middle of the three PWP transducers on the bottom of the flume, a ball was laid so that it connected with a linear displacement transducer through a wire. During test, the ball buried in the sample moves together with the sample; in this manner, the time series of sliding distance can be monitored. To ensure that the ball would move together with the sample without relative motion, a styrene foam ball 2 cm in diameter and 0.1g in weight was adopted, and a 160-g counterweight was attached to the other end of the wire to balance the pulling resistance of the linear-displacement transducer. Because of the resolution of this large capacity (150 cm) linear displacement transducer, displacements smaller than 1.5 mm cannot be measured correctly. Therefore, to get precise measurement, a laser displacement sensor with resolution of 0.015 mm and capacity of 15 mm was also used by fixing a target on the wire and shining a laser beam upon the target. Above the flume two spray-nozzles were placed, and a uniform artificial rainfall was assured. Three video cameras were used to monitor the entire test process from both sides and the downstream front view of the flume.

In the flume tests, water was first added to the oven-dried samples to make the initial water content rise up to 5 percent, and then the sand was stirred evenly. After that, the sample was packed into the flume with an inclination of 30 degrees (see Fig. 6). To make the sample uniform, while packing, the sample was placed in a series of layers of 2 cm thickness parallel to the flume base, and then each layer was tamped. Finally, the superfluous parts of placed sample were removed and the shape was made to be as shown in Fig. 6. Initial dry density was determined from the oven-dried weight of the used mass and the volume of the sample.

4. Results and discussion

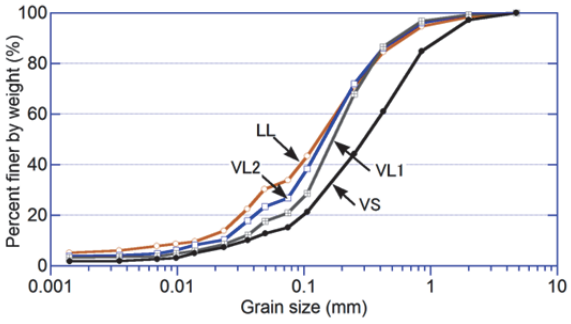

Fig. 7. Grain size distribution

The grain size distributions of these samples are presented in Fig. 7, where it is noticed that LL has finest grains, VS is the coarsest, while VL1 and VL2 locate between them VS and LL. The SEM photos

revealed that LL shows a loose structure with fines attaching on the surface of coarse grains (Fig. 8a), while VS has fewer fines on the surface of coarse grains, but has big air holes in the coarse grains (Fig. 8b), which probably had been formed due to the bust-out of gas and steam during the eruption.

Undrained ring shear tests were performed on all the four samples, and results showed liquefaction phenomenon can be triggered in all the tests. Fig. 9 gives an example of the test on saturated VL1. The sample was consolidated under a normal stress of 60 kPa and shear stress of 38 (corresponding to a slope angle of 32 degrees), and then was sheared under undrained condition by increasing the shear stress to trigger failure. It is noticed that after failure, the measured shear stress presents the shear resistance of the soil. As seen in Fig. 9, with increasing of shear stress, pore water pressure (PWP) increased. After failure, the PWP showed a sharp increase, and shear resistance lowered to a very small value (almost zero), and the PWP reached almost the same value of normal stress, i.e., full liquefaction was initiated.

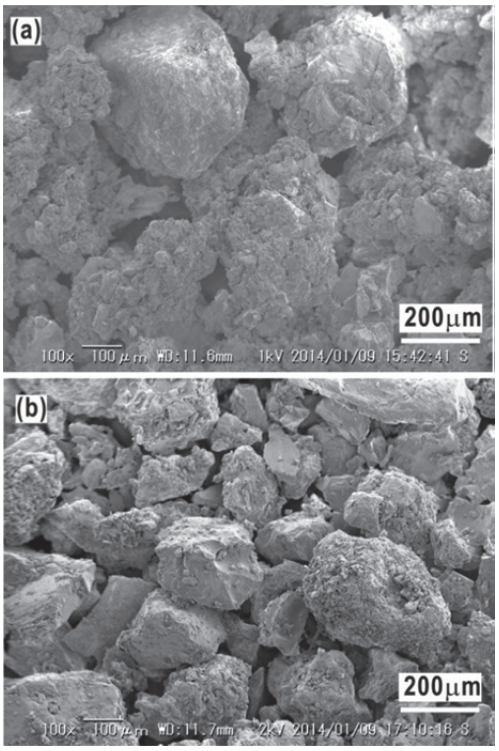

Fig. 8 SEM photos of sample LL and VS

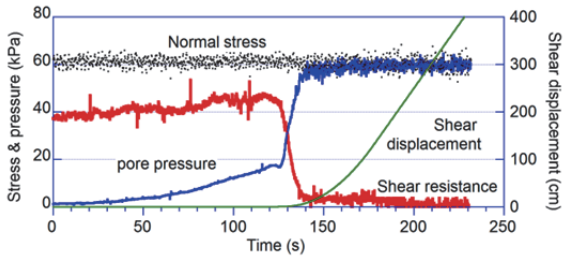

Fig. 9 Undrained shear test on saturated volcanic deposit

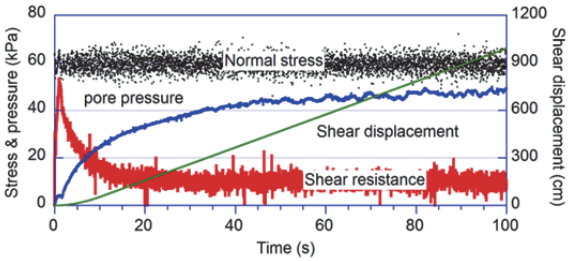

Fig. 10 Shear test on M15-saturated volcanic deposit under partially drained condition (initial density: 1.44 g/cm^3)

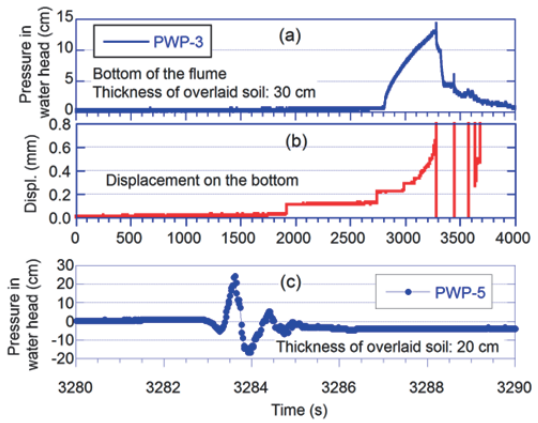

Fig. 11 Pore-water pressure (PWP-3) and displacement on the bottom and PWP within sliding mass after failure in flume test

The results of partially drained shear tests on the M15-fluid-saturated sample are presented in Fig. 10 in the form of time series data. As shown, less PWP was built up before the shear failure occurred. However, after the shear failure PWP increased continuously with progress of shear displacement, and increased to a high value, and the shear resistance lowered to a small value (about 10 kPa) at the time of 20 second, thereafter remained approximately as a constant. The continued increasing in monitored PWP might result from the fact that shearing is localized on within the shear zone where high PWP might be built up, however, the transducers to measure the PWP were located outside of the shear zone. This difference in location would result in the delay in the measured data. From Fig. 10, we infer that the landsliding with long travel distance could be triggered if the saturated soil layer above the sliding surface is thick enough such that the dissipation of generated excess pore-water pressure from the shear zone can be retarded.

Retrogressive failure phenomena occurred in the rainfall-triggered landslides in flume. Although there are some small differences in each test due to the difference in initial density of the soil layer, these retrogressive failures were characterized by slow deformation with small displacement, and then

followed by quick downslope movement. Fig. 11 gives an example of monitored water pressures within the soil layer and displacement along the base of the soil layer. It is seen that small displacement occurred at the time of around 2000 second, there was a small increase in the water pressure. The main failure occurred at the rainfall duration of around 2700s. During the main failure, water pressure showed quick increase with fast movement. However, a detailed examine on the PWP transducer P5 revealed that P5 showed a temporal reduce in PWP and then followed by increase of PWP. This might result from the fact that during the failure moment, the upper soil layer suffered tension deformation due to the retrogressive failure, while the upper soil layer was still in unsaturated state. This was verified by the monitored moistures at different soil depth. Fig. 12 presents the variation of soil moistures of soil layers at differing locations. After 60 minutes of rainfall, the moistures at differing locations increased with further continuing of rainfall, but had different response. M3 at the bottom of the soil layer on the toe part had the greatest value. This indicates that the soil layers on other areas were not in the fully saturated state. After failure, compression might have occurred within the soil layer, resulting further increase in the moisture content and generation of higher PWP. These test results as shown in Figs. 11-12 show that due to the infiltration of rainwater, ground water level above the sliding surface will be elevated such that failure can be initiated within the soil layer, and at the movement of failure, the upper soil layers are not fully saturated. Nevertheless, the displaced materials can suffer from movement with high mobility.

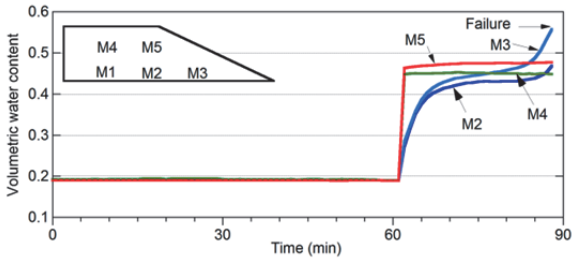

Fig. 12 Water content of soil layers at different locations

5. Conclusions

The principal findings could be summarized as follows:

(1) The Motomachi DA occurred along the boundary between the loess layer and overlaying tephra (Y2.0) that were formed during the volcanic eruption in 1684. The lower permeability of loess layer could lead to the formation of a peached saturated zone above it, and then result in the instability of this hillside.

(2) The meteorological data and the forest state on the slope suggest that strong wind might also have played an important role in triggering the instability of hillside in large area.

(3) High pore-water pressure can be built up after the occurrence of slope failure, and then reduce the shear resistance, even if the shallow soil layer were under partially drained condition.

(4) The displaced landslide materials can suffer from rapid movement even if surficial soil layers were at unsaturated state. Once shear failure occurred, high pore-water pressure can be built up and maintained with delayed dissipation.

Acknowledgements

This work was supported by MEXT KAKENHI (Grant Number: 25900002). Discussions and help in the field trips given by many group members participating in this KAKENHI are greatly appreciated.

References

Geospatial Information Authority of Japan (2013): Public release of aerial photographs showing disaster areas damaged from a landslide caused by heavy rain due to typhoon No.26, 2013. In: http://www.gsi.go.jp/kokusaikoryu/kokusaikoryu-e30023.html

Geological Survey of Japan (2013): The geological background of the shallow landslides triggered by the November 16, 2013 typhoon Wipha on the west part of Izu Oshima. In: https://www.gsj.jp/hazards/landslide/131016oshima.html (accessed on May 15, 2015)

Hungr, O., Evans, S.G, Bovis, M. and Hutchinson, J.N. (2001): Review of the classification of landslides of the flow type. Environmental and Engineering Geoscience, VII, pp. 221-238.

Ishihara, K. (1993): Liquefaction and flow failure during earthquakes. Géotechnique, 43 (3), 349-451.

Kawanabe, Y. (1998): Geological map of Izu-Oshima volcano. Geological map of volcanoes, Geological Survey of Japan, 1998 (in Japanese with English Abstract).

Koyama, M. and Hayakawa, Y. (1996): Syn- and post-caldera eruptive history of Izu Oshima volcano based on tephra and loess stratigraphy. Journal of Geography, 105, 133-162.

Terajima, T., Matsushi, Y., and Hattanji, T. (2014): Hydrological aspects to shallow landslide occurrence in Izu-Oshima Island, triggered by a heavy rainfall of Typhoon 26th on October 15-16, 2013. Annuals of Disas. Prev. Res. Inst., Kyoto Univ., No. 57A: 17-24.